

# Quantum spin liquids in frustrated spin-1 diamond antiferromagnets

Finn Lasse Buessen,<sup>1</sup> Max Hering,<sup>2</sup> Johannes Reuther,<sup>2,3</sup> and Simon Trebst<sup>1</sup>

<sup>1</sup>*Institute for Theoretical Physics, University of Cologne, 50937 Cologne, Germany*

<sup>2</sup>*Dahlem Center for Complex Quantum Systems and Institut für Theoretische Physik, Freie Universität Berlin, Arnimallee 14, 14195 Berlin, Germany*

<sup>3</sup>*Helmholtz-Zentrum Berlin für Materialien und Energie, Hahn-Meitner-Platz 1, 14019 Berlin, Germany*  
(Dated: May 8, 2022)

Motivated by the recent synthesis of the spin-1 A-site spinel  $\text{NiRh}_2\text{O}_4$ , we investigate the classical to quantum crossover of a frustrated  $J_1$ - $J_2$  Heisenberg model on the diamond lattice upon varying the spin length  $S$ . Applying a recently developed pseudospin functional renormalization group (pf-FRG) approach for arbitrary spin- $S$  magnets, we find that systems with  $S \geq 3/2$  reside in the classical regime where the low-temperature physics is dominated by the formation of coplanar spirals and a thermal (order-by-disorder) transition. For smaller local moments  $S=1$  or  $S=1/2$  we find that the system evades a thermal ordering transition and forms a quantum spiral spin liquid where the fluctuations are restricted to characteristic momentum-space surfaces. For the tetragonal phase of  $\text{NiRh}_2\text{O}_4$ , a modified  $J_1$ - $J_2^-$ - $J_2^\perp$  exchange model is found to favor a conventionally ordered Néel state (for arbitrary spin  $S$ ) even in the presence of a strong local single-ion spin anisotropy and it requires additional sources of frustration to explain the experimentally observed absence of a thermal ordering transition.

In the field of frustrated magnetism, spinel compounds of the form  $\text{AB}_2\text{X}_4$  (with  $\text{X}=\text{O}, \text{Se}, \text{S}$ ) have long been appreciated as a source of novel physical phenomena [1]. B-site spinels with magnetic B ions and non-magnetic A ions, such as  $\text{ACr}_2\text{O}_4$  or  $\text{AV}_2\text{O}_4$  (with  $\text{A}=\text{Mg}, \text{Zn}, \text{Cd}$ ), realize pyrochlore antiferromagnets where geometric frustration manifests itself in a vastly suppressed ordering temperature relative to the Curie-Weiss temperature. Conceptually, the pyrochlore Heisenberg antiferromagnet is a paradigmatic example of a three-dimensional spin liquid [2, 3], in both its classical [4, 5] and quantum [6, 7] variants. A-site spinels, with non-magnetic B ions and magnetic A ions forming a diamond lattice, have caught broader attention some ten years ago with the synthesis of  $\text{MnSc}_2\text{S}_4$  [8],  $\text{FeSc}_2\text{S}_4$  [8], and  $\text{CoAl}_2\text{O}_4$  [9, 10] that, similar to the B-site spinels, exhibit a dramatic suppression of their ordering temperature. At first sight counterintuitive due to the unfrustrated nature of the diamond lattice, it was conceptualized [11] that a sizable next-nearest neighbor coupling (connecting spins on the fcc sublattices of the diamond lattice) induces strong geometric frustration. Indeed it could be shown that the classical Heisenberg model with both nearest and next-nearest neighbor exchange

$$\mathcal{H} = J_1 \sum_{\langle i,j \rangle} \mathbf{S}_i \mathbf{S}_j + J_2 \sum_{\langle\langle i,j \rangle\rangle} \mathbf{S}_i \mathbf{S}_j, \quad (1)$$

exhibits highly-degenerate coplanar spin spiral ground states for antiferromagnetic  $J_2 > |J_1|/8$ . Describing a single coplanar spin spiral by a momentum vector  $\vec{q}$  (indicating its direction and pitch), the degenerate ground-state manifold can be captured by a set of  $\vec{q}$  vectors that span a “spin spiral surface” in momentum space [11] as illustrated in Fig. 1. While these spiral surfaces bear a striking resemblance to Fermi surfaces [12], they are considerably more delicate objects that can be easily destroyed by small perturbations to the Hamiltonian (1) (such as further interactions) or even by fluctuations [11, 13] that will induce an order-by-disorder transition into a simple magnetically ordered state (typically captured by a single  $\vec{q}$  vector). Such a description of the magnetism of A-site spinels in terms of classical local moments has proved sufficient to

capture the physics of the Mn and Co-based spinels [11, 14–16] with local moments  $S=5/2$  and  $S=3/2$ , respectively, while the physics of  $\text{FeSc}_2\text{S}_4$  ( $S=2$ ) is dominated by the formation of a spin-orbit coupled local moment [17, 18].

Earlier this year, the synthesis of the first spin-1 A-site spinel has been reported –  $\text{NiRh}_2\text{O}_4$ , which is found to exhibit no thermal ordering transition down to 0.1 K [19], possibly indicating the formation of a quantum spin liquid ground state. This motivates us to consider the *quantum* version of the minimal exchange model (1) for spins of arbitrary length  $S$  in this manuscript and ask whether qualitatively new physics arises in the crossover from the classical to the quantum regime (upon decreasing the spin length). We work with a pseudo-fermion functional renormalization group (pf-FRG) approach [20] that has proved capable of handling competing interactions and emergent spin liquid physics in three-dimensional, frustrated quantum magnets [21–23] and which has recently been generalized to spin- $S$  systems [24]. Our numerical results indicate that a distinct classical to quantum crossover occurs for spin  $S = 3/2$ . While the low temperature physics is dominated, independent of the spin length  $S$ , by the formation

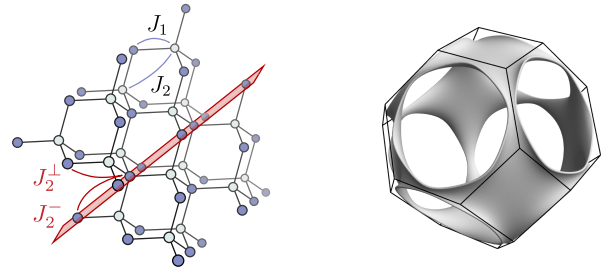


FIG. 1. **Frustrated diamond lattice antiferromagnet.** Left: Diamond lattice with nearest ( $J_1$ ) and next-nearest neighbor coupling ( $J_2$ ). A tetragonal distortion of the lattice along one spatial axis (orthogonal to the plane indicated in red) splits the 12 next-nearest neighbor couplings into a group of 4 in-plane terms ( $J_2^\perp$ ) and 8 out-of-plane terms ( $J_2^\parallel$ ). Right: Spin spiral surface for  $J_2/|J_1| = 0.73$  plotted in the first Brillouin zone (solid lines).

of spin spiral correlations that manifest themselves in the spin structure factor in the form of clearly discernible spin spiral surfaces (akin to the one shown in the right panel of Fig. 1), we find that only for systems with spin  $S \geq 2$  do these correlations proliferate and give rise to a thermal phase transition into a magnetically ordered ground state. For systems with spin  $S \leq 1$  we find no indication of a thermal phase transition for the full extent of the spiral regime  $J_2/J_1 > 1/8$ . The system with  $S = 3/2$  is found to sit precisely at the border with no thermal phase transition occurring in the regime  $1/8 < J_2/J_1 \lesssim 0.4$  and a thermal phase transition into a magnetically ordered ground state for  $J_2/J_1 \gtrsim 0.4$ . For the spin-1 system of interest in the context of  $\text{NiRh}_2\text{O}_4$  these findings support the notion that quantum fluctuations paired with strong geometric frustration can indeed prevent the formation of magnetic ordering and that the system remains fluctuating amongst different spin spiral states down to the zero temperature. However, when considering a slightly modified exchange model with two distinct types of next-nearest neighbor exchanges that has been proposed [19] for the tetragonal phase of  $\text{NiRh}_2\text{O}_4$  we find that this picture no longer holds. In fact, we find that the modified energetics strongly inhibit the spin spiral fluctuations and instead favor the formation of conventional Néel order for arbitrary spin length  $S$ . We will return to this point towards the end of the manuscript and discuss how to possibly consolidate these findings with the experimental absence of a thermal phase transition.

**Pseudofermion FRG.**— To explore the exchange model (1) we employ the pf-FRG approach [20], which recasts the original spin degrees of freedom in terms of auxiliary Abrikosov fermions and then applies the well-developed FRG approach of fermionic systems [25]. In the language of the original spin model, the pf-FRG approach amounts to a concurrent  $1/S$  and  $1/N$  expansion that allows to faithfully capture conventionally ordered magnetic states (typically favored already in the large- $S$  limit of the expansion) and spin liquid states (favored in the alternate large- $N$  limit) and is known to become exact in the separate limits of large  $S$  [24] and large  $N$  [26]. With the computational effort scaling quadratically with system size  $\mathcal{O}(N_L^2)$  and quartically with the number of frequencies  $\mathcal{O}(N_\omega^4)$ , there is a trade-off in choosing larger system sizes versus finer energy/temperature resolution. With a focus on the finite-temperature ordering tendencies in the RG flow, we have opted in our numerical simulations for a very finely spaced frequency mesh of 144 frequencies (in a logarithmic spacing) and a system size of  $L = 10$  lattice bonds in every spatial direction (with a total of  $N_L = 981$  sites) resulting in a total number of 24,219,720 differential equations to be integrated for every choice of coupling parameters. An important aspect of the pf-FRG approach is that it can capture the formation of spin spirals with *arbitrary*  $\vec{q}$ -vectors and is not limited by finite-size discretizations.

**Phase diagram.**— A common starting point for the analysis of a pf-FRG calculation is to plot the magnetic susceptibility as a function of frequency cutoff  $\Lambda$  as shown in Fig. 2 for the exchange model (1) at fixed coupling  $J_2/|J_1| = 0.73$  (relevant to  $\text{NiRh}_2\text{O}_4$ ) and varying spin length  $S$ . For small spins  $S=1/2$  and  $S=1$  the susceptibility follows a smooth trajectory down

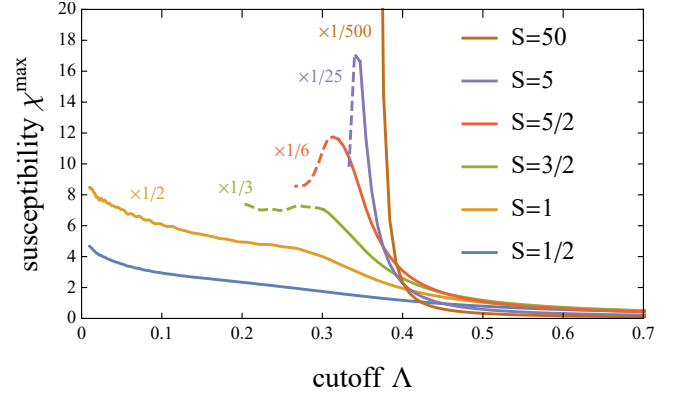


FIG. 2. **Flow of susceptibility** for different spin lengths  $S$  for fixed couplings  $J_2/|J_1| = 0.73$ . The energy scale is normalized by spin length and coupling strength, such that the flow breakdown occurs at similar scales. The susceptibility is always plotted at the momentum-space location where it is maximal.

to the lowest temperature and there is no obvious breakdown of the RG flow, which is typically interpreted as the absence of any magnetic ordering transition. Contrarily, for spins  $S=3/2$  and larger the RG flow exhibits a clear breakdown that signals the onset of magnetic order. In fact, what is only a kink in the flow at  $S=3/2$  becomes a true divergence in the classical limit ( $S=50$ ). We note that the critical cutoff  $\Lambda_c$  [27] at which the flow breaks down slightly shifts towards larger values for increasing spin length indicating a stronger ordering tendency as one approaches the classical limit.

Identifying the critical cutoff  $\Lambda_c$  with a transition temperature  $T_c = \Lambda_c \pi/2$  [21, 22], we can map out, for this classical regime, a finite-temperature phase diagram as illustrated for  $S=5/2$  (relevant e.g. to  $\text{MnSc}_2\text{S}_4$ ) in Fig. 3. The phase diagram shows a smooth evolution of the (unnormalized) transition temperature for increasing next-nearest neighbor coupling  $J_2$  and fixed nearest neighbor coupling  $J_1 = -1$  [28].

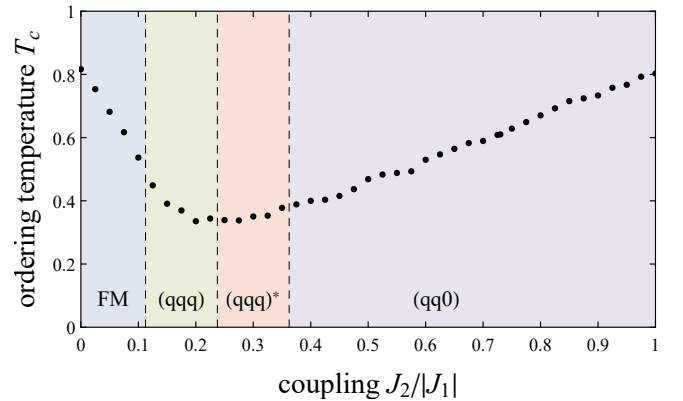


FIG. 3. **Finite-temperature phase diagram.** Shown is the transition temperature versus the coupling ratio  $J_2/|J_1|$  for spin  $S = 5/2$ . The background shadings indicate the different types of ground-state order, see the ground-state phase diagram of Fig. 6.

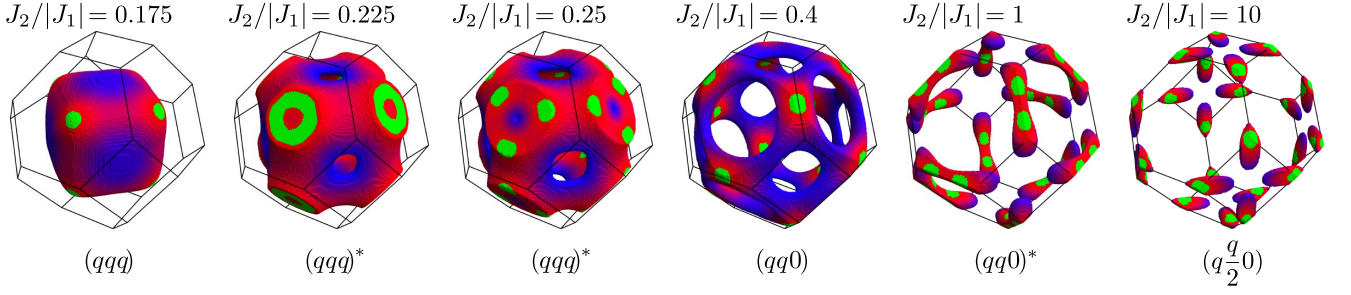


FIG. 5. **Spin structure factor of the spin-1 model for varying coupling  $J_2/|J_1|$ .** Depicted are the top 20% of the spin structure factor at frequency cutoff  $\Lambda = 0$  with the same color coding applied as in Fig. 4. The spin structure factor shows sharp surface-like features whose evolution with  $J_2$  reflects the spin spiral surface found in the ground state of the classical  $J_1$ - $J_2$  exchange model [11]. The maxima (indicated in green) indicate an incipient magnetic ordering at wavevectors  $(qqq) \rightarrow (qqq)^* \rightarrow (qq0) \rightarrow (qq0)^* \rightarrow (q\frac{q}{2}0)$  for increasing  $J_2$ . Note that since the maximum of the structure factor is typically hidden inside the finite extent of the depicted manifold (see the right panel of Fig. 4 for an illustration) we project the maximum radially onto the surface of the manifold.

Similar to Monte Carlo results [11] for the classical exchange model, we find a significant suppression of the transition temperature for  $1/8 \lesssim J_2/|J_1| \lesssim 0.4$ , i.e. upon entering the spin spiral regime.

To explore the onset of magnetic ordering it is highly instructive to track the evolution of the spin structure factor in the RG flow. This is illustrated for the spin-1 model in Fig. 4 below where for fixed coupling  $J_2/|J_1| = 0.73$  we plot the top 20% of the spin structure factor and the color code reflects the relative strength – blue is low, red is high, and green is the top 0.4%. For large cutoff  $\Lambda$  the system fluctuates widely among many different possible magnetic orderings which is reflected in a momentum-space structure factor that is broadly spread out in the Brillouin zone. In the low-temperature, small cutoff regime, however, we find that the features of the spin structure factor sharpen considerably and become highly reminiscent of the spin spiral surface found for the ground state of the classical  $J_1$ - $J_2$  exchange model [11]. This is visualized for the spin-1 model for various values of the coupling ratio  $J_2/|J_1|$  in Fig. 5 above. Ignoring the coloring scheme for a moment, one sees that the spin structure factor indeed retraces the spin spiral surface evolving from a spherical object for small  $1/8 < J_2/|J_1| \lesssim 0.2$  to an open surface that touches the border of the Brillouin zone and forms holes around the  $(qqq)$ -direction for larger  $J_2$  to more line-like objects first around the  $(qq0)$  direction for  $J_2/|J_1| \approx 1$  to two crossing line-like objects in the large  $J_2$  limit. These observations fall in line with results for the spin structure factor of the classi-

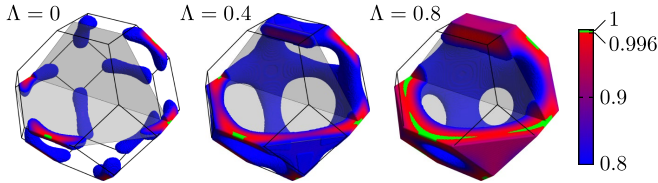


FIG. 4. **Evolution of the spin structure factor** with frequency cutoff  $\Lambda$  for coupling  $J_2/|J_1| = 0.73$  and spin  $S = 1$ . The colored regions mark the top 20% of the structure factor. Blue corresponds to 80% of the maximum value, red to 99.6%. The top 0.4% are colored green.

cal exchange model obtained from Monte Carlo simulations that similarly reveal the spin spiral surface in the vicinity of the finite-temperature transition [11]. Here our focus is on further discerning the subset of points within the spiral surface where the structure factor is maximally enhanced, which provides an indicator of the magnetic ordering that will proliferate in case of a thermal phase transition and determine the ground state order. Tracking these points one finds that beyond the Néel / ferromagnetic state for vanishing  $J_2$  the preferred ordering momenta go for increasing  $J_2$  through a sequence  $(qqq) \rightarrow (qqq)^* \rightarrow (qq0) \rightarrow (qq0)^* \rightarrow (q\frac{q}{2}0)$  (where the asterisk marks an ordering direction around a high-symmetry direction).

Repeating this analysis for varying spin length  $S$  allows us to map out the general ground-state phase diagram of Fig. 6 as a function of both the coupling ratio  $J_2/|J_1|$  and spin length  $S$ . We find that the general evolution of the spiral surface and the sequence of incipient ordering momenta do not change upon going from the quantum regime ( $S=1/2$ ) deep into the

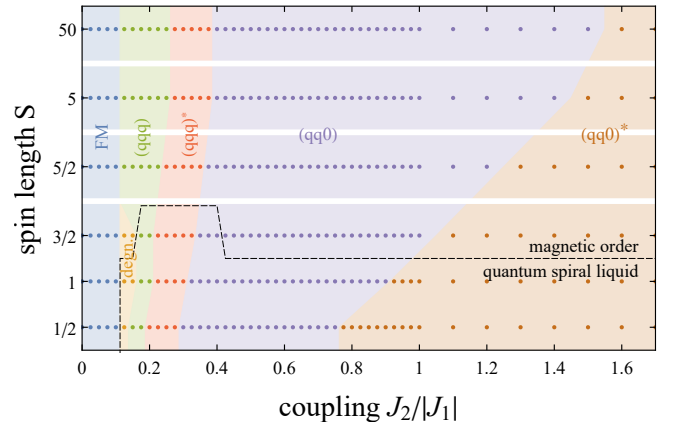


FIG. 6. **Ground state phase diagram.** The zero-temperature magnetic ordering (indicated by the coloring) as a function of the coupling ratio  $J_2/|J_1|$  and spin lengths varying from the quantum limit  $S = 1/2$  (bottom) to the classical limit  $S = 50$  (top).



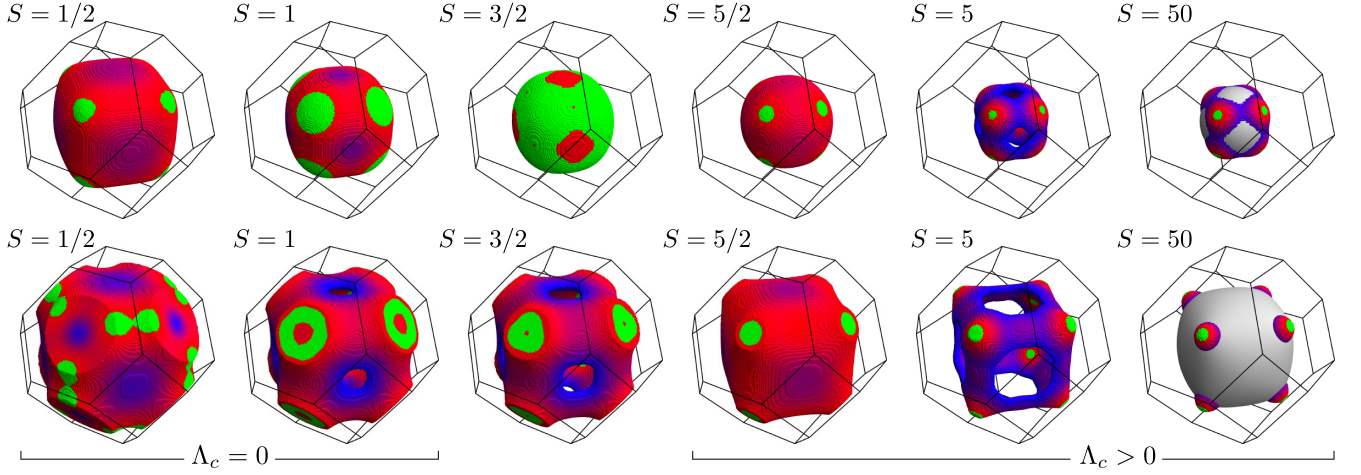


FIG. 7. **Effect of quantum fluctuations for varying spin length.** Depicted are the top 20% of the spin structure factor at the lowest frequency cutoff (either zero or right above the ordering transition) with the same color coding applied as in Fig. 4. The top panel is for  $J_2/|J_1| = 0.15$ , the bottom panel for  $J_2/|J_1| = 0.225$ . The surface-like features reveal nearly degenerate spiral manifolds akin to the spiral surfaces of the ground state of the classical spin model [11] (indicated by the grey shaded spheres in the last panel). With decreasing spin length the spiral surface notably expands. The maxima (indicated in green) indicate an incipient magnetic ordering. Similar data for  $J_2/|J_1| = 0.35$  and  $J_2/|J_1| = 1$  is shown in Fig. 12 of the appendix.

classical regime ( $S=50$ ) with only the boundary between the  $(qq0)$  and  $(qq0)^*$  order showing a noticeable dependence on the spin length  $S$ .

**Quantum fluctuations.**— With the spin structure factor revealing the spiral surface, i.e. the manifold of approximately degenerate spin spirals at low temperatures, we can now systematically investigate the effect of quantum fluctuations upon varying the spin length  $S$ . To this end, we plot the leading contribution (top 20%) to the spin structure factor in Fig. 7 for fixed  $J_2$  and varying spin length  $S$ . In the classical limit ( $S=50$ ), the spiral surface determined via the spin structure factor maps out a manifold of similar size and shape as found in the Luttinger-Tisza calculation [29, 30] for the ground state of the classical model (indicated by the grey spheres in the panels on the very right). Increasing quantum fluctuations with decreasing spin length  $S$ , the spiral surfaces become not only more pronounced but systematically expand, similar to the trend observed for increasing the geometric frustration by ramping up  $J_2$  in Fig. 5). This expansion can be readily explained by the fact that quantum systems gain more energy from antiferromagnetic fluctuations as opposed to ferromagnetic ones. This expansion of the spiral surface upon decreasing the spin length is also the reason for the shifts of the phase boundaries in the ground-state phase diagram of Fig. 6.

Turning to the evolution of the incipient magnetic order (indicated by the green coloring in Fig. 7) upon varying the spin length, we note that for most spin length  $S$  the maxima of the spin structure factor are well described by singular points or ring-like structures. The spin-3/2 system for  $J_2/|J_1| = 0.15$  (upper row) stands out as the *entire* spherical spiral surface remains degenerate down to  $\Lambda = 0$ . Such a degenerate regime upon entering the spin spiral phase, indicated by the orange shading in the ground-state phase diagram of Fig. 6, has also been reported in earlier  $Sp(N)$  calculations [13].

**Quantum spiral spin liquids.**— The absence of a thermal phase transition (see also Fig. 13 of the appendix) for the low-spin system with  $S=1/2$ ,  $S=1$  and, for a limited parameter regime,  $S=3/2$  points towards the formation of an unconventional ground state. In fact, the system remains fluctuating amongst different spin spiral states down to zero temperature as indicated by a spin structure factor that even for vanishing frequency cutoff  $\Lambda = 0$  reveals a spin spiral surface – akin to the classical systems with  $S \geq 2$  just *above* the transition temperature, see Fig. 7. We dub this heavily fluctuating quantum state a *quantum spiral spin liquid* and note that this is a decisively different state from the quantum paramagnetic [31] ground state recently suggested for the spin-1 system at hand.

**NiRh<sub>2</sub>O<sub>4</sub>.**— Let us finally turn to the spin-1 A-site spinel NiRh<sub>2</sub>O<sub>4</sub> [19], whose recent synthesis has motivated the current study of the spin- $S$   $J_1$ - $J_2$  exchange model (1). NiRh<sub>2</sub>O<sub>4</sub> exhibits strong antiferromagnetic couplings with a Curie-Weiss temperature of  $\Theta_{CW} \approx -10$  K and shows no signs of a magnetic ordering transition down to 0.1 K [19]. While one might hope that this makes NiRh<sub>2</sub>O<sub>4</sub> a prime candidate for the spin liquid physics of frustrated spin-1 diamond antiferromagnets discussed in this manuscript, there are some indications that the exchange model of Eq. (1) needs to be further expanded to truthfully capture the physics of NiRh<sub>2</sub>O<sub>4</sub>. For one, the structural transition of NiRh<sub>2</sub>O<sub>4</sub> requires to adjust the role of next-nearest neighbor couplings. As argued in Ref. [19] one should discriminate between in-plane  $J_2^-$  and out of plane  $J_2^\perp$  next-nearest neighbor couplings as indicated in Fig. 1. Ab initio theory [19] suggests that the relevant coupling strengths for NiRh<sub>2</sub>O<sub>4</sub> are given by  $J_1 = 1$ ,  $J_2^- = 0.73$ ,  $J_2^\perp = -0.91$  with antiferromagnetic  $J_1$ ,  $J_2^-$  and ferromagnetic  $J_2^\perp$ . If, however, we consider these two distinct types of next-nearest neighbor couplings, we find, both in a Luttinger-Tisza calculation for the classical limit as well as in our pf-FRG calcu-

lations for all spin  $S$ , a conventional, Néel ordered ground state that is accompanied by a finite-temperature transition. One possible way to induce a novel source of frustration in the tetragonal phase of  $\text{NiRh}_2\text{O}_4$  is to include a local single-ion spin anisotropy, which has been argued [32] to drive the system into a paramagnetic regime. Indeed, we find in our pf-FRG calculations (where special care has to be taken to assure that the FRG flow remains within the spin-1 subspace, see the Appendix) that the system undergoes a transition into a paramagnetic phase for  $D/J_1 \approx 2$  for the original  $J_1$ - $J_2$  model (see Appendix). This trivial paramagnet where the system effectively decouples into single sites exhibits a *featureless* spin structure factor as opposed to the quantum spiral spin liquid discussed above. For the tetragonal  $J_1$ - $J_2^-$ - $J_2^\perp$  model, however, we find that the Néel ordered ground state remains stable upon including the single-ion spin anisotropy. Up to values of  $D/J_1 \approx 8$  (up to which the pf-FRG calculations are trustworthy) we do not see a transition into the paramagnetic phase. This indicates that it will require additional sources of frustration to explain the apparent absence of a finite-temperature

ordering transition in  $\text{NiRh}_2\text{O}_4$ . Looking ahead, it would be highly desirable to explore the physics of  $\text{NiRh}_2\text{O}_4$  using neutron diffraction experiments such as the ones recently undertaken for  $\text{MnSc}_2\text{S}_4$  demonstrating that the scattering data can indeed reveal the spin spiral surface [16].

## ACKNOWLEDGMENTS

We thank J. Attig for providing us with the Luttinger-Tisza result for the classical limit of the modified exchange model for  $\text{NiRh}_2\text{O}_4$ . This work was partially supported by the DFG within the CRC 1238 (project C02) and Transregio CRC 183 (project A02). The numerical simulations were performed on the CHEOPS cluster at RRZK Cologne and the JURECA cluster at the Forschungszentrum Juelich. J.R. is supported by the Freie Universität Berlin within the Excellence Initiative of the German Research Foundation. F.L.B. thanks the Bonn-Cologne Graduate School of Physics and Astronomy (BCGS) for support.

- 
- [1] H. Takagi and S. Niitaka, Highly frustrated magnetism in spinels, in *Introduction to Frustrated Magnetism: Materials, Experiments, Theory*, edited by C. Lacroix, P. Mendels, and F. Mila (Springer Berlin Heidelberg, Berlin, Heidelberg, 2011) pp. 155–175.
  - [2] L. Balents, Spin liquids in frustrated magnets, *Nature* **464**, 199 (2010).
  - [3] L. Savary and L. Balents, Quantum spin liquids: a review, *Reports on Progress in Physics* **80**, 016502 (2017).
  - [4] R. Moessner and J. T. Chalker, Properties of a Classical Spin Liquid: The Heisenberg Pyrochlore Antiferromagnet, *Phys. Rev. Lett.* **80**, 2929 (1998).
  - [5] R. Moessner and J. T. Chalker, Low-temperature properties of classical geometrically frustrated antiferromagnets, *Phys. Rev. B* **58**, 12049 (1998).
  - [6] B. Canals and C. Lacroix, Pyrochlore Antiferromagnet: A Three-Dimensional Quantum Spin Liquid, *Phys. Rev. Lett.* **80**, 2933 (1998).
  - [7] B. Canals and C. Lacroix, Quantum spin liquid: The Heisenberg antiferromagnet on the three-dimensional pyrochlore lattice, *Phys. Rev. B* **61**, 1149 (2000).
  - [8] V. Fritsch, J. Hemberger, N. Büttgen, E.-W. Scheidt, H.-A. Krug von Nidda, A. Loidl, and V. Tsurkan, Spin and Orbital Frustration in  $\text{MnSc}_2\text{S}_4$  and  $\text{FeSc}_2\text{S}_4$ , *Phys. Rev. Lett.* **92**, 116401 (2004).
  - [9] N. Tristan, J. Hemberger, A. Krimmel, H.-A. Krug von Nidda, V. Tsurkan, and A. Loidl, Geometric frustration in the cubic spinels  $M\text{Al}_2\text{O}_4$  ( $M = \text{Co}, \text{Fe}, \text{and Mn}$ ), *Phys. Rev. B* **72**, 174404 (2005).
  - [10] T. Suzuki, H. Nagai, M. Nohara, and H. Takagi, Melting of antiferromagnetic ordering in spinel oxide  $\text{CoAl}_2\text{O}_4$ , *Journal of Physics: Condensed Matter* **19**, 145265 (2007).
  - [11] D. Bergman, J. Alicea, E. Gull, S. Trebst, and L. Balents, Order-by-disorder and spiral spin-liquid in frustrated diamond-lattice antiferromagnets, *Nat Phys* **3**, 487 (2007).
  - [12] J. Attig and S. Trebst, Classical Spin Spirals in Frustrated Magnets from Free-Fermion Band Topology, *arXiv:1705.04073*.
  - [13] J.-S. Bernier, M. J. Lawler, and Y. B. Kim, Quantum Order by Disorder in Frustrated Diamond Lattice Antiferromagnets, *Phys. Rev. Lett.* **101**, 047201 (2008).
  - [14] S. Lee and L. Balents, Theory of the ordered phase in *A*-site antiferromagnetic spinels, *Phys. Rev. B* **78**, 144417 (2008).
  - [15] L. Savary, E. Gull, S. Trebst, J. Alicea, D. Bergman, and L. Balents, Impurity effects in highly frustrated diamond-lattice antiferromagnets, *Phys. Rev. B* **84**, 064438 (2011).
  - [16] S. Gao, O. Zaharko, V. Tsurkan, Y. Su, J. S. White, G. S. Tucker, B. Roessli, F. Bourdarot, R. Sibille, D. Chernyshov, T. Fennell, A. Loidl, and C. Ruegg, Spiral spin-liquid and the emergence of a vortex-like state in  $\text{MnSc}_2\text{S}_4$ , *Nat Phys* **13**, 157 (2017).
  - [17] G. Chen, L. Balents, and A. P. Schnyder, Spin-Orbital Singlet and Quantum Critical Point on the Diamond Lattice:  $\text{FeSc}_2\text{S}_4$ , *Phys. Rev. Lett.* **102**, 096406 (2009).
  - [18] G. Chen, A. P. Schnyder, and L. Balents, Excitation spectrum and magnetic field effects in a quantum critical spin-orbital system: The case of  $\text{FeSc}_2\text{S}_4$ , *Phys. Rev. B* **80**, 224409 (2009).
  - [19] J. R. Chamorro and T. M. McQueen, Frustrated  $S = 1$  On A Diamond Lattice, *arXiv:1701.06674*.
  - [20] J. Reuther and P. Wölfe,  $J_1$ - $J_2$  frustrated two-dimensional Heisenberg model: Random phase approximation and functional renormalization group, *Phys. Rev. B* **81**, 144410 (2010).
  - [21] Y. Iqbal, R. Thomale, F. Parisen Toldin, S. Rachel, and J. Reuther, Functional renormalization group for three-dimensional quantum magnetism, *Phys. Rev. B* **94**, 140408 (2016).
  - [22] F. L. Buessen and S. Trebst, Competing magnetic orders and spin liquids in two- and three-dimensional kagome systems: Pseudofermion functional renormalization group perspective, *Phys. Rev. B* **94**, 235138 (2016).
  - [23] Y. Iqbal, T. Müller, K. Riedl, J. Reuther, S. Rachel, R. Valentí, M. J. P. Gingras, R. Thomale, and H. O. Jeschke, Signatures of a gearwheel quantum spin liquid in a spin- $\frac{1}{2}$  pyrochlore molybdate Heisenberg antiferromagnet, *arXiv:1705.05291*.
  - [24] M. L. Baez and J. Reuther, Numerical treatment of spin systems with unrestricted spin length  $S$ : A functional renormalization group study, *arXiv:1612.05074*.
  - [25] C. Wetterich, Exact evolution equation for the effective poten-

tial, Physics Letters B **301**, 90 (1993).

- [26] D. Roscher *et al.*, in preparation.  
 [27] Note that we have rescaled all energy scales in the manuscript by a factor of  $2S\sqrt{J_1^2 + J_2^2}$ .  
 [28] The choice of *ferromagnetic* nearest neighbor coupling  $J_1$  is primarily motivated to simplify the discussion of the structure factor data (by restricting it to the 1st Brillouin zone). In general, we find that the quantum system is, similarly to its classical counterpart, largely insensitive to the sign of the nearest neighbor coupling.

- [29] J. M. Luttinger, A Note on the Ground State in Antiferromagnetics, Phys. Rev. **81**, 1015 (1951).  
 [30] J. M. Luttinger and L. Tisza, Theory of Dipole Interaction in Crystals, Phys. Rev. **70**, 954 (1946).  
 [31] C. Wang, A. Nahum, and T. Senthil, Topological paramagnetism in frustrated spin-1 Mott insulators, Phys. Rev. B **91**, 195131 (2015).  
 [32] G. Chen, Quantum Paramagnet and Frustrated Quantum Criticality in a Spin-One Diamond Lattice Antiferromagnet, arXiv:1701.05634.

## Appendix A: Spin-S consistency checks

*Large-S generalization.*— The generalization of pf-FRG flow equations to larger spins  $S \geq 1$  is constructed by a substitution of the spin operators by artificial moments  $\mathbf{S}_i = \sum_{\kappa=1}^{2S} \mathbf{S}_{i\kappa}$  as discussed in detail in Ref. [24]. To ensure projection into the correct subspace of the resulting spin algebra, all spin flavors  $\kappa$  must align ferromagnetically. This can be energetically enforced by introducing an additional level repulsion term into the Hamiltonian (1)

$$\mathcal{H}' = \mathcal{H} + A \sum_i \left( \sum_{\kappa=1}^{2S} \mathbf{S}_{i\kappa} \right)^2 \quad (\text{A1})$$

and choosing  $A < 0$ . The same level repulsion term also guarantees single occupation of Abrikosov fermions, even for spin-1/2 systems.

Numerical data for varying strength of level repulsion  $A < 0$  are shown in Fig. 8. Note that the depicted susceptibility flows remain largely invariant upon introducing a small, finite level repulsion. This indicates that the fermion filling constraints are readily fulfilled in pf-FRG calculations even in the absence of the level repulsion and the spin-S generalization does indeed hold.

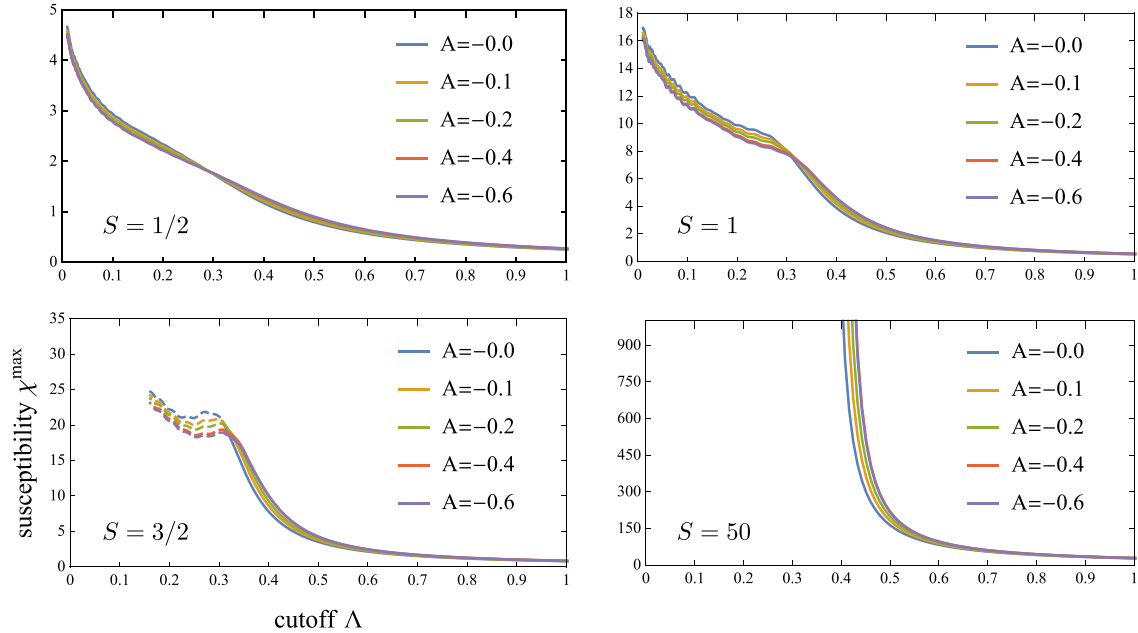


FIG. 8. **Level repulsion term in spin-S calculations.**  $J_1$ - $J_2$  Heisenberg model at  $J_2/|J_1| = 0.73$  with finite level repulsion  $A < 0$ . The data has been rescaled to a common energy scale by a factor of  $2S\sqrt{J_1^2 + J_2^2} + A^2$  such that all data sets coalesce to a single curve.

## Appendix B: Local spin anisotropy

To explore possible alternative sources of frustration, we consider a local (single-ion) spin anisotropy in addition to the Heisenberg interactions

$$\mathcal{H}' = \mathcal{H} + D \sum_i S_i^z S_i^z - A \sum_i \mathbf{S}_i \mathbf{S}_i, \quad (\text{B1})$$

where  $D > 0$  parametrizes the strength of the anisotropy. Note that within the pf-FRG scheme for spins  $S > 1/2$ , the anisotropy term may not only drive the system into the  $S_i^z = 0$  sector, but it could just as well drive the system into the unphysical  $\mathbf{S}_i = 0$  sector. To constrain the system to the physical sector we need to carefully counterbalance the spin anisotropy term with a level repulsion term (see previous section). Since the spin anisotropy term can be recast as  $S_i^z S_i^z = \mathbf{S}_i \mathbf{S}_i - S_i^x S_i^x - S_i^y S_i^y$ , which includes a contribution of the same form as the level repulsion term, it is apparent that the strength of the level repulsion should be at least  $A/D > 1$ .

If we first consider the single-ion limit  $D \rightarrow \infty$  we find that the in and out-of-plane susceptibilities converge in a range of  $3 \lesssim A/D \lesssim 10$  as shown in Fig. 9, though we note that the out-of-plane susceptibility never vanishes entirely. For large level repulsion strength  $A/D \gtrsim 10$  the susceptibilities start to diverge indicating a breakdown of the pf-FRG framework.

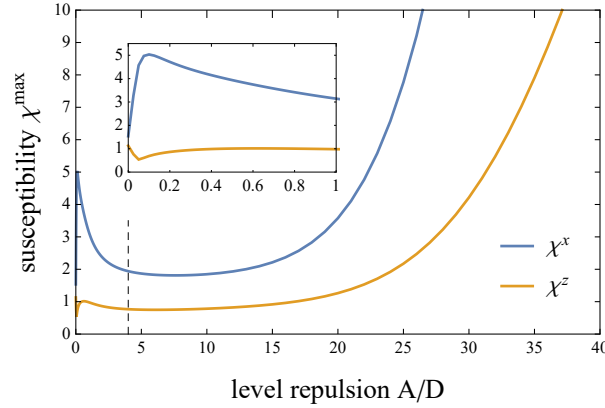


FIG. 9. **Local spin anisotropy for a single ion.** The susceptibility of a single spin-1 moment at zero cutoff plotted for different ratios of the anisotropy  $D$  and the counter-balancing level repulsion term  $A$ . At small level repulsion ( $A/D \lesssim 3$ ) contributions from the unphysical sector of the Hilbert space dominate as well as for very large level repulsion ( $A/D \gtrsim 10$ ). In between there exists a flat plateau where the system is constrained to the physical Hilbert space.

In Figs. 10 and 11 we show the in and out-of-plane susceptibility flows for varying strengths of the local spin anisotropy both for the original  $J_1$ - $J_2$  Heisenberg model (for  $J_2/|J_1| = 0.73$ ) as well as the tetragonal  $J_1$ - $J_2^-$ - $J_2^\perp$  model, respectively. For the spiral spin liquid of the  $J_1$ - $J_2$  Heisenberg model we see the expected crossover to the trivial paramagnet of the large  $D$  limit at around  $D/|J_1| \approx 2$  in accordance with the mean-field estimates of Ref. [32]. For the tetragonal model, on the other hand, we do not observe such a transition up to values of  $D/|J_1| \approx 8$  as illustrated in Fig. 11.

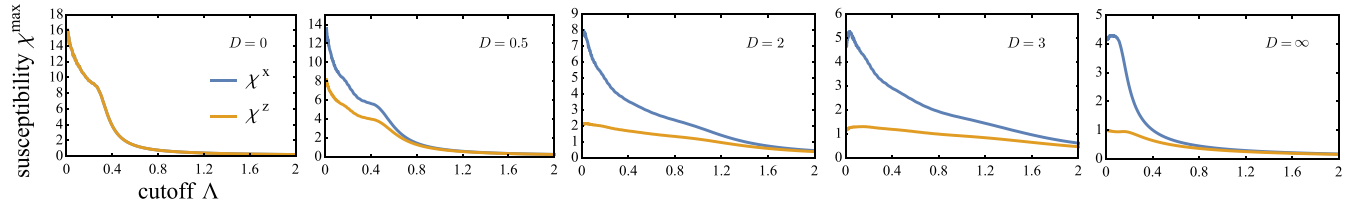


FIG. 10. **Spin anisotropy in the  $J_1$ - $J_2$  Heisenberg model** at  $J_2/|J_1| = 0.73$  and different values for the anisotropy  $D$ . The level repulsion term  $A$  is chosen such that  $A/D = 4$  for all values of  $D$ .

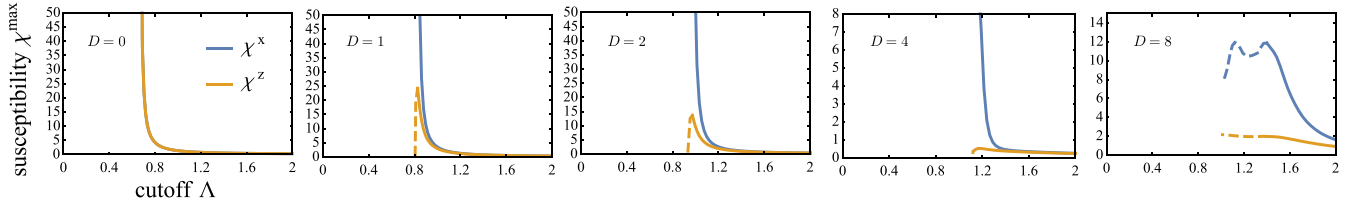


FIG. 11. **Spin anisotropy in the  $J_1$ - $J_2^-$ - $J_2^\perp$  model** with coupling constants as suggested in ab initio calculations [19] and an additional spin anisotropy  $D$ . The level repulsion term  $A$  is chosen such that  $A/D = 4$  for all values of  $D$ .

### Appendix C: Supplemental data

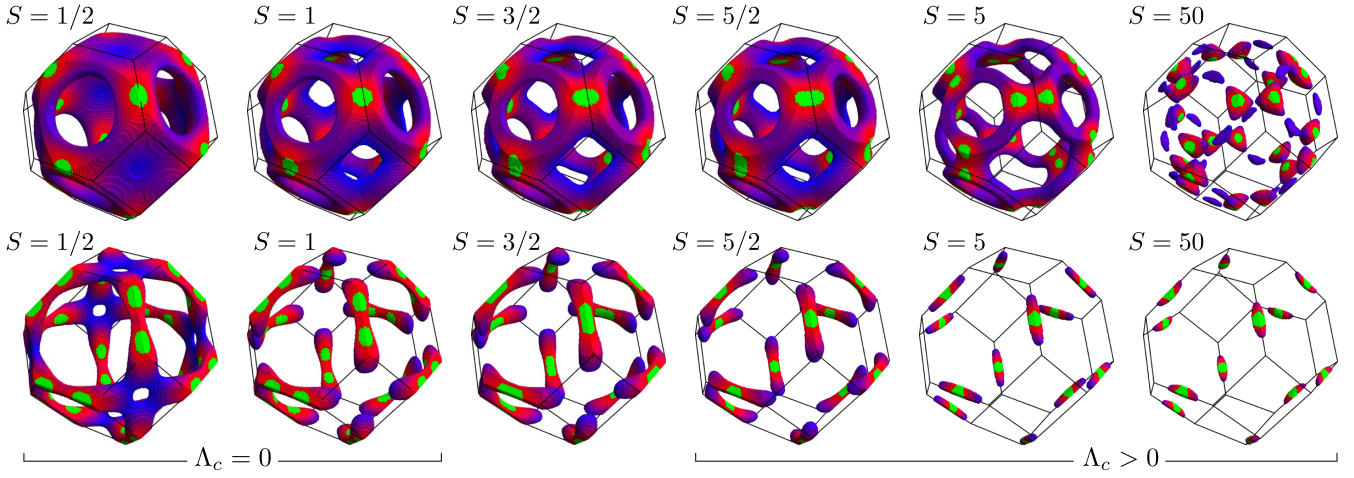


FIG. 12. **Effect of quantum fluctuations for varying spin length.** Same as Fig. 7 but for couplings  $J_2/|J_1| = 0.35$  (top row) and  $J_2/|J_1| = 1$  (bottom row).



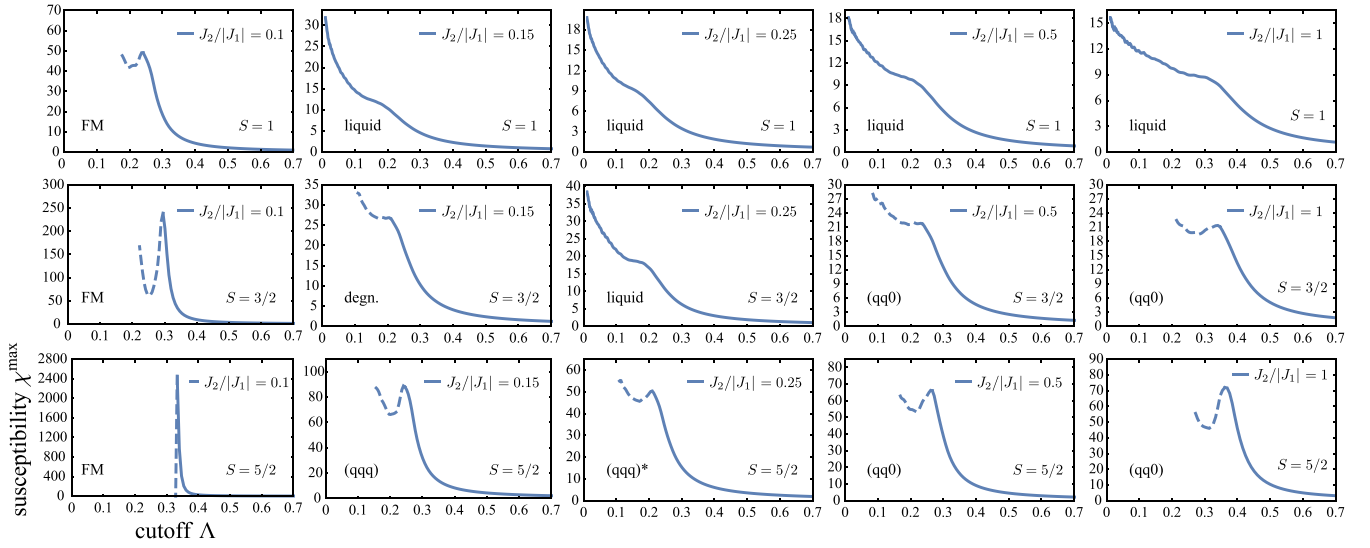


FIG. 13. **Flow of the spin susceptibility** for various coupling strengths  $J_2/|J_1|$  (columns) and varying  $S$  (rows). Shown here is the maximum of the susceptibility versus frequency cutoff  $\Lambda$  for the exchange model (1) with  $S=1$  (top row),  $S=3/2$  (middle row), and  $S=5/2$  (bottom row).